

## Supplementary information

### Wet flue gas CO<sub>2</sub> capture and utilization using one-dimensional metal-organic chains

Chiu, Nan Chieh;<sup>a</sup> Loughran, Ryan P.;<sup>a</sup> Gładysiak, Andrzej;<sup>b</sup> Vismara, Rebecca;<sup>c</sup> Park, Ah-Hyung Alissa;<sup>b</sup> Stylianou, Kyriakos C.\*<sup>a</sup>

<sup>a</sup>Materials Discovery Laboratory (MaD Lab), Department of Chemistry, Oregon State University, Corvallis, Oregon, United States

Email. [kyriakos.stylianou@oregonstate.edu](mailto:kyriakos.stylianou@oregonstate.edu)

<sup>b</sup>Department of Earth and Environmental Engineering, Department of Chemical Engineering, Lenfest Center for Sustainable Energy, Columbia University, New York, United States

<sup>c</sup>Departamento de Química Inorgánica, Universidad de Granada, 18071 Granada, Spain

## Materials Synthesis

$[\text{Ni}_3(\text{pzdc})_2(\text{ade})_2(\text{H}_2\text{O})_{1.5}]\cdot(\text{H}_2\text{O})_{1.3}$  was synthesized based on previous reports with slightly modifications.<sup>1</sup> The mixture of  $\text{NiCO}_3$  (48 mg, 0.404 mmol), 3,5-pyrazoledicarboxylic acid ( $\text{H}_3\text{pzdc}$ ) (47 mg, 0.270 mmol) and adenine ( $\text{Hade}$ )(40 mg, 0.296 mmol) in 8 mL deionized water (DI water) for 96 hours at 140 °C (cooling down rate: 0.1 °C/min). The blue crystals were then filtered and washed with DI water three times.

## Characterization

**The powder X-ray diffraction** patterns (PXRD) were recorded by using a Bruker D8 Advance diffractometer, which is equipped for monochromatic Cu K $\alpha$  radiation ( $\lambda=1.5418 \text{ \AA}$ ) at 40 kV and 25 mA. The setting of the scanning condition were as following: scan speed: 0.2 seconds per step, step size:  $0.02^\circ$  in  $2\theta$ ,  $2\theta$  range: 3–35°, and under ambient temperature.

**Thermogravimetric analyses (TGA)** were operated with a standard Thermogravimetry/Differential Thermal Analysis (TG-DTA) analyzer. The temperature range was from 30 °C to 650 °C with a heating rate of 10 °C/min under air flow (100 mL/min).

**Single component adsorption-desorption isotherms** were collected at specific temperatures ( $\text{N}_2$ : 77 and 298 K;  $\text{CO}_2$ : 273, 298, and 303 K; Water: 298 K) up to 1 bar using a Micromeritics 3FLEX apparatus and ASAP 2020. For water isotherm analyses, the different water vapor pressures were controlled by a Micromeritics temperature controller. By altering the temperature, water can be evaporated at different vapor pressures, which were subsequently used to dose the sample

**Temperature dependence UV-visible absorbance** was obtained using a PerkinElmer UV-visible spectrometer equipped with an integrating sphere. The diffuse reflectance was collected by depositing the powders within a high-temperature reaction chamber solid sample holder, and loading that into the Praying Mantis. The Harrick temperature

controller and water chiller were used for changing the temperature from 25 °C to 300 °C. The Kubelka-Munk (K-M) function was applied to the raw spectral data.

**Chemical stability analysis** was carried out by washing the solid material after catalytic reaction and dried in the oven at 75 °C overnight for PXRD analysis.

**Fourier Transform Infrared Spectroscopy (FTIR) spectra** were collected at room temperature with a Perkin Elmer Spectrum Two Spectrometer equipped with a LiTaO<sub>3</sub> MIR detector. The scanning range was from 4000 to 450 cm<sup>-1</sup> at a 4 cm<sup>-1</sup> resolution for 4 accumulated scans each.

### Breakthrough Experiments

Breakthrough curves were recorded using the fixed-bed reactor setting. A sample of [Ni<sub>3</sub>(pzdc)<sub>2</sub>(ade)<sub>2</sub>(H<sub>2</sub>O)<sub>4</sub>](H<sub>2</sub>O)<sub>1.3</sub> was introduced into a glass tube with 1.3 cm inner diameter with a heater tape wound on it and supported with some glass wool. For the purpose of adsorbent activation, the sample was heated under He (40 cm<sup>3</sup>/min) at 383 K for certain time (15 min, 1.5h, 2h, and 3h), and then cooled down to 298 K. Upon temperature stabilization, [Ni<sub>3</sub>(pzdc)<sub>2</sub>(ade)<sub>2</sub>](H<sub>2</sub>O)<sub>0.4</sub> was exposed to the gas mixture composed of 15 vol% CO<sub>2</sub> and 85% of N<sub>2</sub>. Simultaneously with the onset of exposure, the CO<sub>2</sub> breakthrough curve started being recorded with a Horiba IR gas analyzer. The CO<sub>2</sub> capacity was calculated using the ideal gas approximation (Equation 1).

$$q_{\text{CO}_2} = \frac{C_{\text{CO}_2} p \dot{V} (t_{\text{sample}} - t_{\text{beads}})}{m_{\text{ads}} R T} \quad (\text{Eq.1})$$

where:  $q_{\text{CO}_2}$  = CO<sub>2</sub> capacity [mol/g],  $C_{\text{CO}_2}$  = Volume fraction of CO<sub>2</sub> in the feed gas = 0.15,  $p$  = Pressure = 1.013 10<sup>5</sup> Pa,  $\dot{V}$  = Volume flow rate [cm<sup>3</sup>/s],  $t$  = Dynamic adsorption time [s],  $m_{\text{ads}}$  = Mass of the adsorbent [g],  $R$  = 8.31 10<sup>6</sup> Pa·cm<sup>3</sup>/(mol·K),  $T$  = Temperature = 298 K

In Equation 2, the dynamic adsorption time recorded with non-adsorbent glass beads,  $t_{\text{beads}}$ , was subtracted from the dynamic adsorption time recorded with the adsorbent

sample,  $t_{\text{sample}}$ , for the purpose of blank correction. Each of these dynamic adsorption times  $t$  was derived from the numerical integration of the relevant breakthrough curve (Equation 2).

$$t = \int_0^{400\text{s}} \left( 1 - \frac{C_\tau}{C_{\text{CO}_2}} \right) d\tau \quad (\text{Eq. 2})$$

where  $C_\tau$  = volume fraction of  $\text{CO}_2$  at the outlet at the time  $\tau$ , probed every 1 s.

Humid gas adsorption on dry MOF was employed to assess the selectivity of  $[\text{Ni}_3(\text{pzdc})_2(\text{ade})_2] \cdot (\text{H}_2\text{O})_{0.4}$  towards  $\text{CO}_2$  over  $\text{H}_2\text{O}$ . The feed gas (15 vol%  $\text{CO}_2$ , 75% of  $\text{N}_2$ ) was humidified up to the relative humidity (RH) of 75% with a gas sparger prior to introduction into the reactor. To protect the gas analyzer, the outlet gas was dried using a Perma Pure nafion tube gas dryer.

### IAST calculations

A 15/85 mol %  $\text{CO}_2/\text{N}_2$  was used to mimic the composition of post combustion flue gas. We calculated the  $\text{CO}_2/\text{N}_2$  selectivity of  $[\text{Ni}_3(\text{pzdc})_2(\text{ade})_2] \cdot (\text{H}_2\text{O})_{0.4}$  based on the method reported by Simon *et al.* with slight modifications.<sup>2</sup> Ideal adsorption solution theory (IAST) and experimental data of  $\text{CO}_2$  and  $\text{N}_2$  isotherm at 298 K were used for  $\text{CO}_2/\text{N}_2$  selectivity computations. As shown in Figure 3a, the  $\text{CO}_2$  isotherm at 298 K showed Type I behavior which can be modeled by the Interpolator Isotherm. For the  $\text{N}_2$  isotherm at 298 K, the maximum uptake of  $\text{N}_2$  is 0.22 mmol/g at 737 mbar which is lower than the  $\text{CO}_2$  uptake at 298 K. Using the Interpolator Isotherm to calculate the  $\text{CO}_2/\text{N}_2$  selectivity led to fitting failure and therefore, Langmuir model was used for fitting the  $\text{N}_2$  isotherm at 298 K.

The selectivity was calculated by using (Equation 3):

$$S_{\text{CO}_2/\text{N}_2} = \frac{X_{\text{CO}_2}/P_{i\text{CO}_2}}{X_{\text{N}_2}/P_{i\text{N}_2}} \quad (\text{Eq. 3})$$

Where  $P_{i\text{CO}_2}$  and  $P_{i\text{N}_2}$  are the mole fractions of  $\text{CO}_2$  and  $\text{N}_2$  (which is 0.15 and 0.85 in

our case), respectively.  $X_{\text{CO}_2}$  and  $X_{\text{N}_2}$  are the  $\text{CO}_2$  and  $\text{N}_2$  gas uptake of  $[\text{Ni}_3(\text{pzdc})_2(\text{ade})_2] \cdot (\text{H}_2\text{O})_{0.4}$  based on the calculation of IAST for 15/85 mol %  $\text{CO}_2/\text{N}_2$  under different total gas pressure.

### Catalysis Experiments

$[\text{Ni}_3(\text{pzdc})_2(\text{ade})_2(\text{H}_2\text{O})_4] \cdot (\text{H}_2\text{O})_{1.3}$  (0.0145 mmol) was added in the stainless autoclave reactor (Parr Instruments Series 4790) with the mixture of propylene oxide (PO) (0.25 mL, 3.57 mmol), tetrabutylammonium bromide (TBAB) (100 mg, 0.31 mmol), and 1,2-dimethoxyethane (DME) (1.75 mL, 16.9 mmol). Then, the reactor was pressurized to 10 bar with pure  $\text{CO}_2$  and heated at 100 °C for optimized time. After finishing the reaction, water bath was used to cool the reactor down to room temperature for 30 minutes and depressurized.

### NMR Spectra and Qualification

The calculation of the yield of propylene carbonate (PC) was followed Le *et al.*<sup>3</sup> A 25  $\mu\text{L}$  aliquot was taken from the reaction solution and diluted with 580  $\mu\text{L}$  of deuterated chloroform in a standard 5 mm NMR tube. A 500 MHz Bruker Avance 500 equipped with a BBO probe was used for  $^1\text{H}$  NMR spectra data collection.

The ring protons of PC and the protons of DME were considered for the PC yield calculation. The data used for sample calculations below are in relation to Figure S1.

To begin with, the ratio of propylene carbonate to DME was calculated from area integrals obtained by NMR.

$$\frac{M_{\text{carbonate}}}{M_{\text{DME}}} = \left( \frac{I_{\text{carbonate}}}{I_{\text{DME}}} \right) \left( \frac{N_{\text{DME}}}{N_{\text{carbonate}}} \right) = \left( \frac{3.02}{56.17} \right) \left( \frac{10}{3} \right) = 0.18$$

(M: Number of mole, N: Number of Nuclei, I=Integral Area)

The molar amount of the solvent, DME, was constant in the reaction. Therefore, the initial molar amount of DME (16.9 mmol) was used as the internal standard for

calculating the amount of PC.

$$M_{\text{carbonate},\text{total}} = \left(\frac{M_{\text{carbonate}}}{M_{\text{DME}}}\right)(M_{\text{DME},\text{total}}) = (0.18)(16.9 \text{ mmol}) = 3.03 \text{ mmol}$$

The yield of the PC can then be calculated by comparing with the amount of PO added in the reaction (3.57 mmol).

$$\text{Yield} = \left(\frac{M_{\text{carbonate},\text{total}}}{M_{\text{PO}}}\right)(100 \%) = \left(\frac{3.03 \text{ mmol}}{3.57 \text{ mmol}}\right)(100 \%) = 84.8 \%$$

## Supplementary Figures

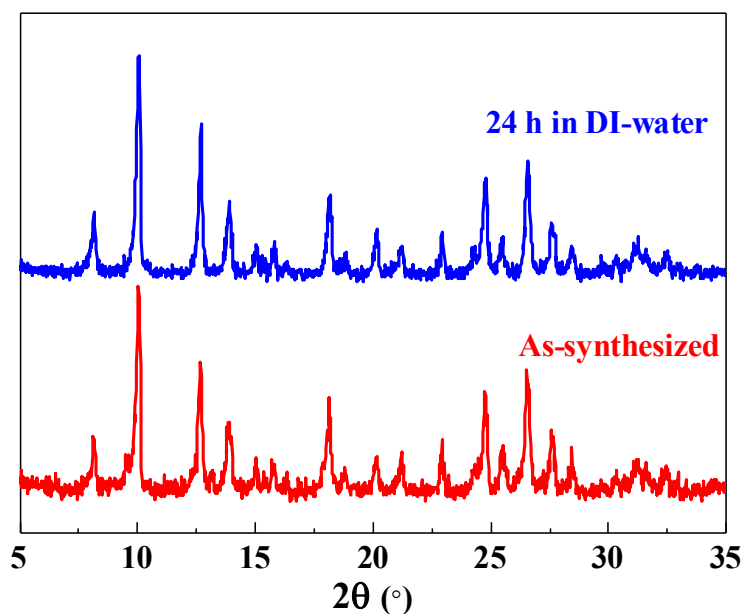


**Figure S1.** PXRD pattern of  $[\text{Ni}_3(\text{pzdc})_2(\text{ade})_2(\text{H}_2\text{O})_{1.5}] \cdot (\text{H}_2\text{O})_{1.3}$  after its immersion in liquid water for 24 h.

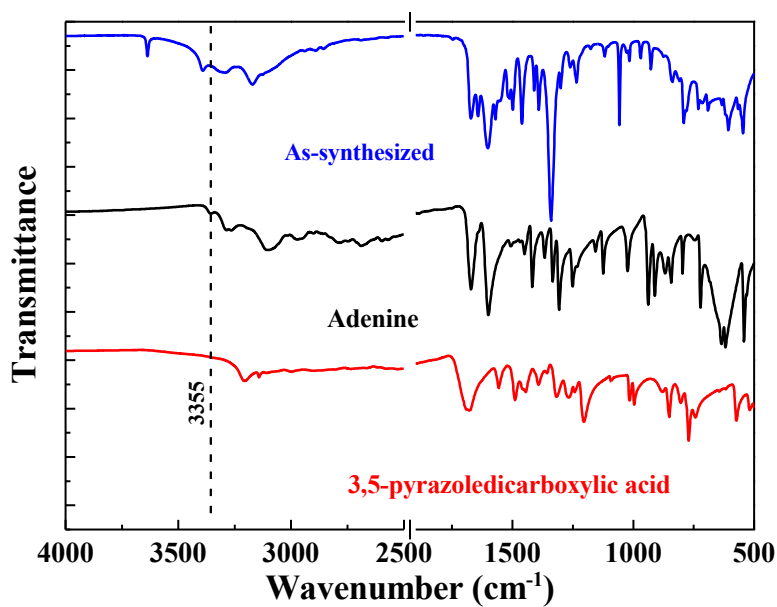


**Figure S2.** FT-IR patterns of (black) adenine, (red) 3,5-pyrazoledicarboxylic acid, and (blue) as-synthesized  $[\text{Ni}_3(\text{pzdc})_2(\text{ade})_2(\text{H}_2\text{O})_4] \cdot (\text{H}_2\text{O})_{1.3}$ . The 3355  $\text{cm}^{-1}$  peak indicates the N-H stretching band.

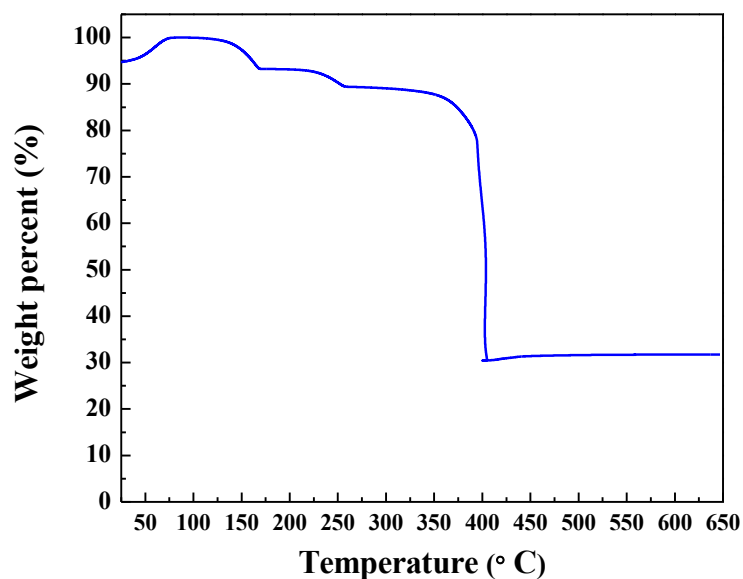


**Figure S3.** TGA pattern of  $\text{Ni}_3(\text{pzdc})_2(\text{ade})_2(\text{H}_2\text{O})_4 \cdot (\text{H}_2\text{O})_{1.3}$ . The first mass losses at 170 °C indicated the removal of guest water molecules and the second mass losses represented the removal of the coordinated water molecules.  $\text{Ni}_3(\text{pzdc})_2(\text{ade})_2(\text{H}_2\text{O})_4 \cdot (\text{H}_2\text{O})_{1.3}$  began to degrade completely at 365 °C.

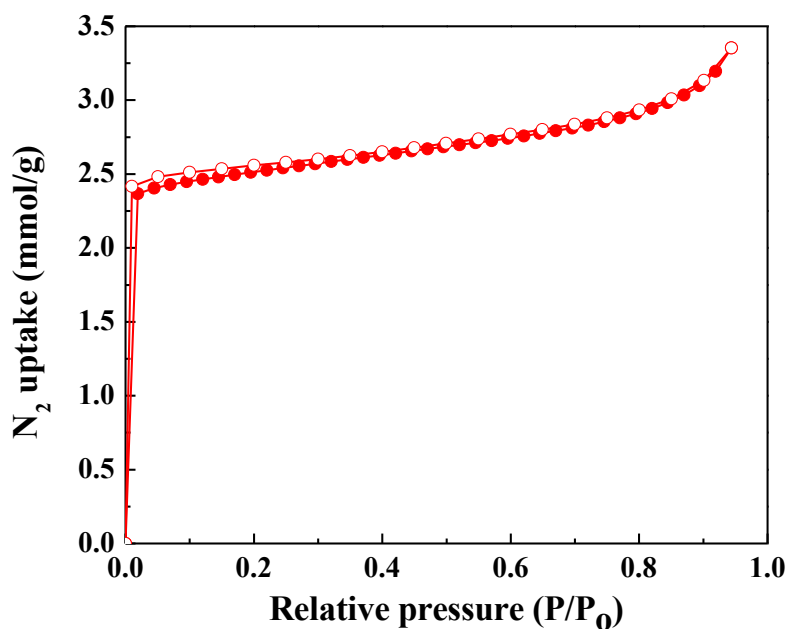


**Figure S4.** Type I nitrogen isotherm for  $[\text{Ni}_3(\text{pzdc})_2(\text{ade})_2] \cdot (\text{H}_2\text{O})_{0.4}$  at 77 K confirms that it is permanently porous. The calculated BET surface area for this MOF is 183  $\text{m}^2/\text{g}$ .

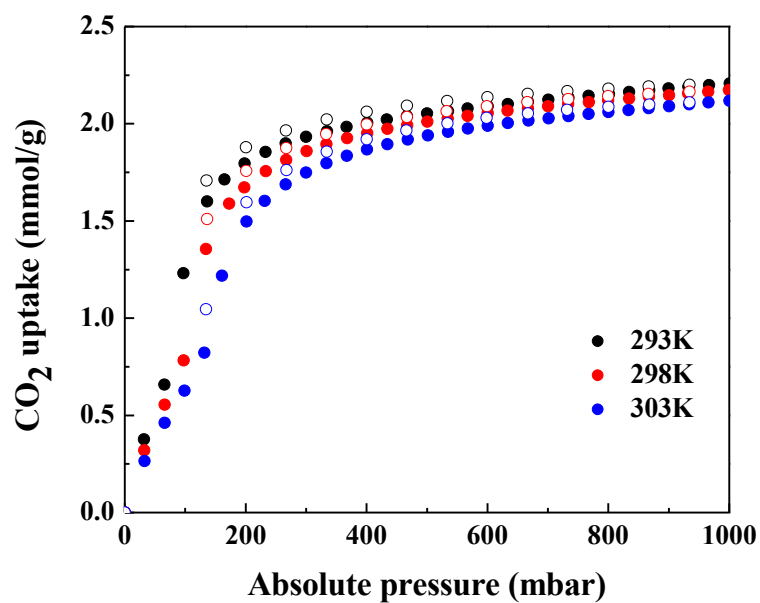


**Figure S5.** CO<sub>2</sub> isotherm patterns of [Ni<sub>3</sub>(pzdc)<sub>2</sub>(ade)<sub>2</sub>](H<sub>2</sub>O)<sub>0.4</sub> at 293 K (black), 298 K (red), and 303 K (blue).

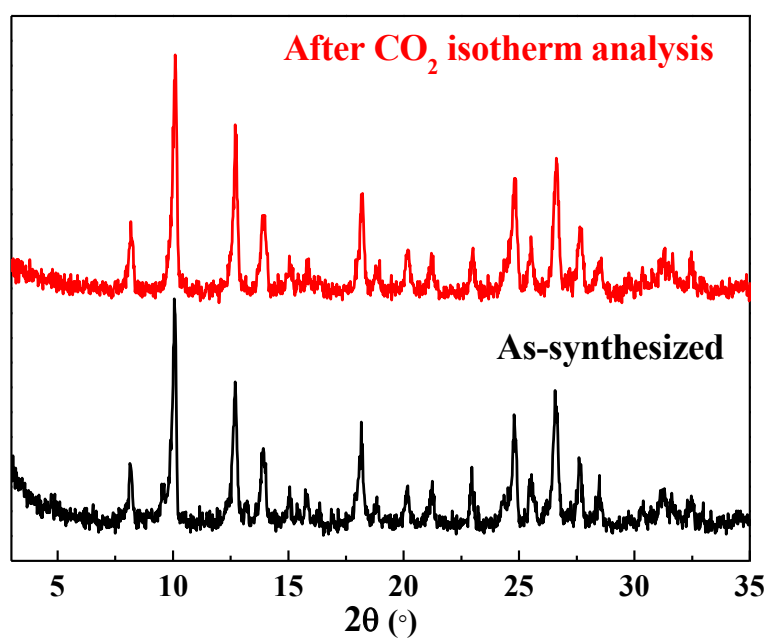


**Figure S6.** PXRD patterns of [Ni<sub>3</sub>(pzdc)<sub>2</sub>(ade)<sub>2</sub>](H<sub>2</sub>O)<sub>0.4</sub> after the CO<sub>2</sub> isotherm analysis at 298 K.

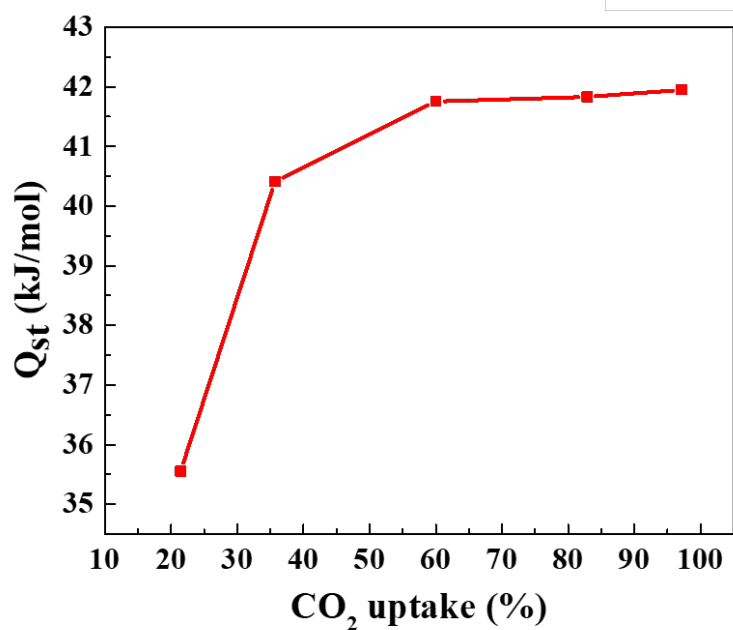


**Figure S7.** Isosteric heat of adsorption ( $Q_{st}$ ) for  $[\text{Ni}_3(\text{pzdc})_2(\text{ade})_2] \cdot (\text{H}_2\text{O})_{0.4}$  towards  $\text{CO}_2$ , calculated using the Clausius-Clapeyron equation using data from the  $\text{CO}_2$  isotherms at 273, 298, and 303 K.

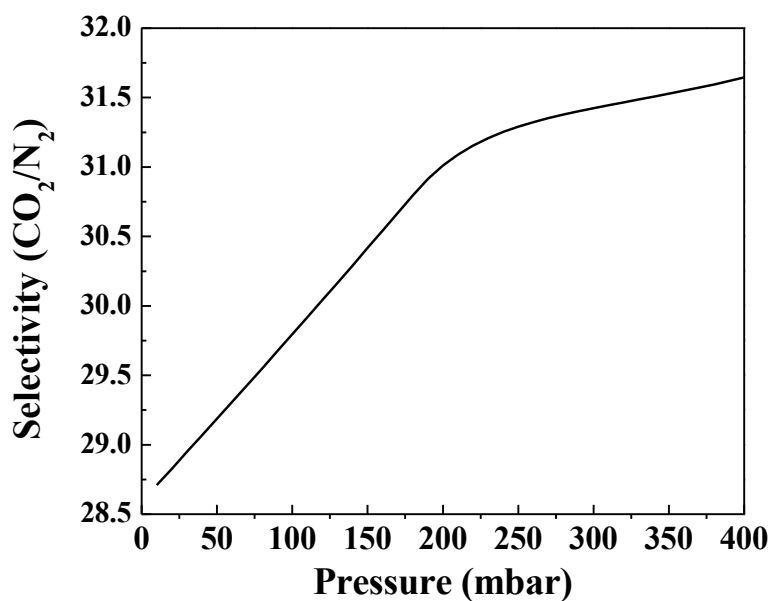


**Figure S8.**  $\text{CO}_2/\text{N}_2$  selectivity pattern of  $[\text{Ni}_3(\text{pzdc})_2(\text{ade})_2] \cdot (\text{H}_2\text{O})_{0.4}$  by Ideal Adsorbed Solution Theory (IAST) simulated mixed-gas adsorption isotherms.

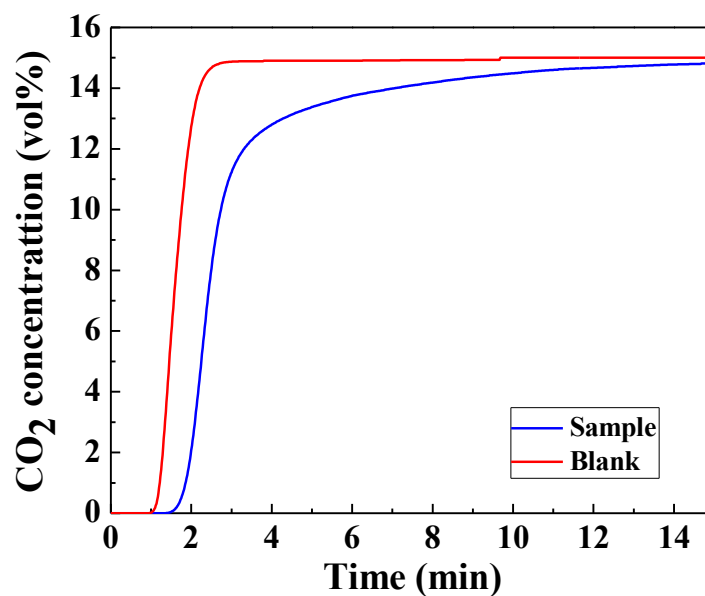


**Figure S9.** Breakthrough curve for dry separation (15% CO<sub>2</sub>: 75% N<sub>2</sub>) with [Ni<sub>3</sub>(pzdc)<sub>2</sub>(ade)<sub>2</sub>](H<sub>2</sub>O)<sub>0.4</sub>. The average CO<sub>2</sub> working capacity under dry conditions is 1.48 mmol/g.

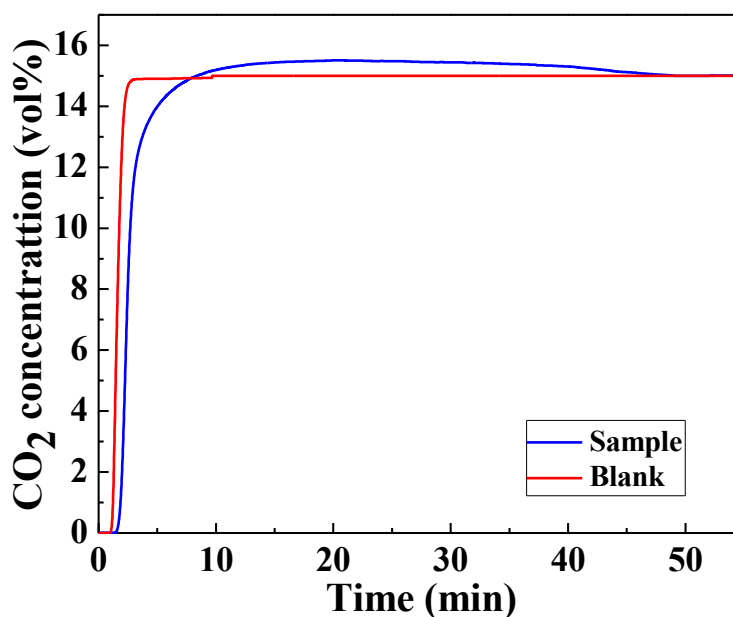


**Figure S10.** Breakthrough curve for humid gas separation (15% CO<sub>2</sub>: 75% N<sub>2</sub>, 75% RH) with [Ni<sub>3</sub>(pzdc)<sub>2</sub>(ade)<sub>2</sub>](H<sub>2</sub>O)<sub>0.4</sub>. The average CO<sub>2</sub> working capacity under humid conditions is 1.09 mmol/g.

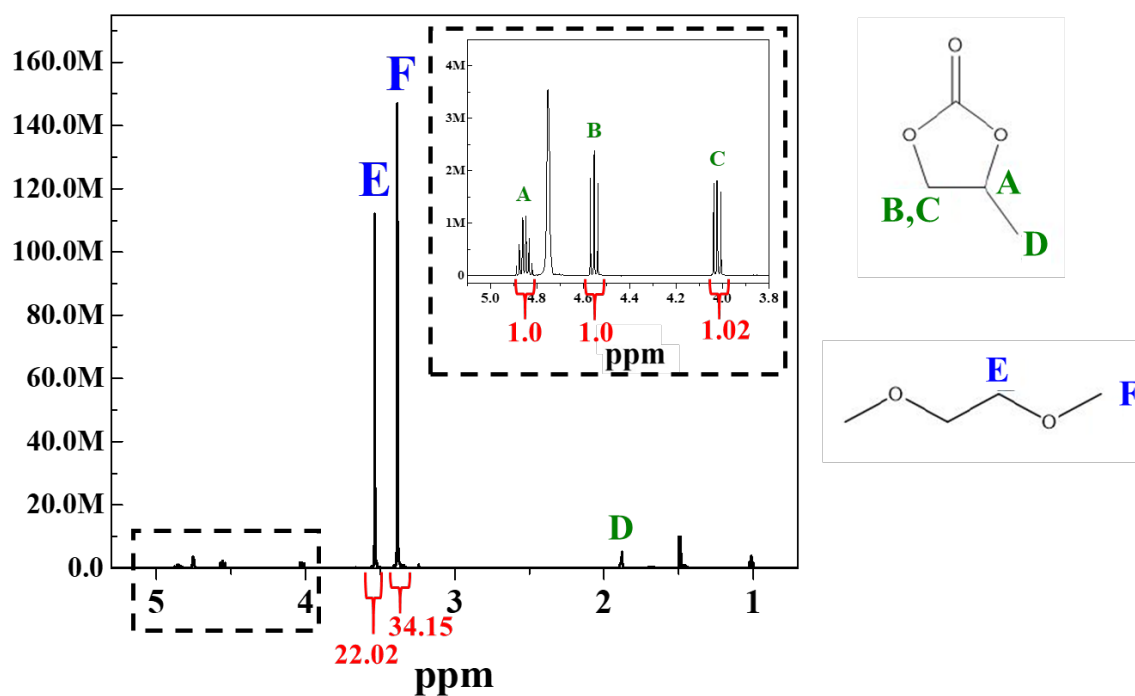


**Figure S11.**  $^1\text{H}$  NMR ( $\text{CDCl}_3$ , 500 MHz) spectra of the catalytic reaction we performed with  $[\text{Ni}_3(\text{pzdc})_2(\text{ade})_2(\text{H}_2\text{O})_4] \cdot (\text{H}_2\text{O})_{1.3}$ . The labeled peaks and their integral area value indicating propylene carbonate (green) and DME (blue). All other residual peaks are due to propylene oxide and TBAB.

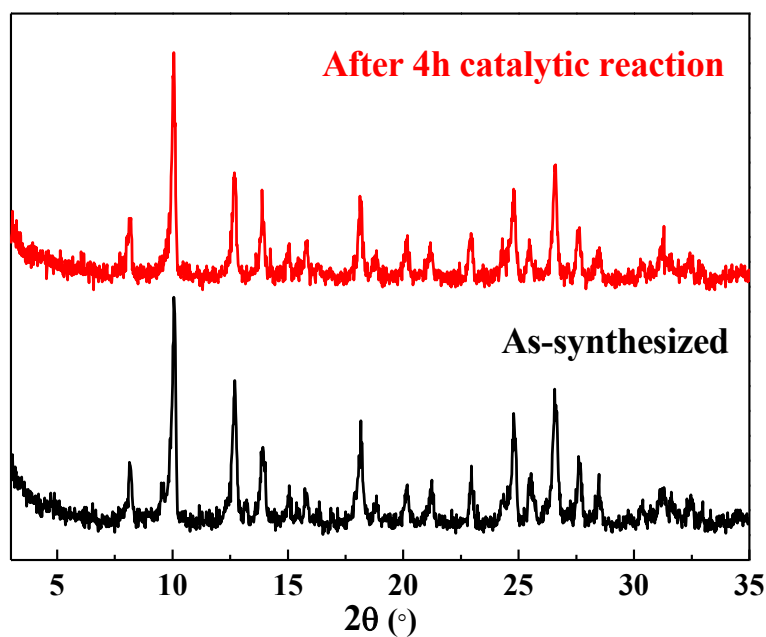


**Figure S12.** PXRD patterns of  $[\text{Ni}_3(\text{pzdc})_2(\text{ade})_2] \cdot (\text{H}_2\text{O})_{0.4}$  after 4 h catalytic reaction under  $100^\circ\text{C}$  and 10 bar pure  $\text{CO}_2$  gas.

**Table S1.** A comparison of materials previously demonstrated for the catalytic addition of CO<sub>2</sub> to propylene oxide for the formation of propylene carbonate. Our material boasts a competitive TOF of 21.95 h<sup>-1</sup> for a 4-hour reaction, with a yield of almost 85%.

Material	Temperature [°C]	CO <sub>2</sub> Pressure [bar]	Time [hr]	TOF [hr <sup>-1</sup> ]	Yield [%]	Reference
[Ni <sub>3</sub> (pzdc) <sub>2</sub> (ade) <sub>2</sub> (H <sub>2</sub> O) <sub>1.5</sub> ](H <sub>2</sub> O) <sub>1.3</sub>	100	10	1	50.93	49.22	This Work
[Ni <sub>3</sub> (pzdc) <sub>2</sub> (ade) <sub>2</sub> (H <sub>2</sub> O) <sub>1.5</sub> ](H <sub>2</sub> O) <sub>1.3</sub>	100	10	2	27.49	53.12	This Work
[Ni <sub>3</sub> (pzdc) <sub>2</sub> (ade) <sub>2</sub> (H <sub>2</sub> O) <sub>1.5</sub> ](H <sub>2</sub> O) <sub>1.3</sub>	100	10	4	21.95	84.94	This Work
[Ce(HTCPB)]	100	2	12	13.4	65.4	3
[Ce(HTCPB)]	100	10	12	20.0	99.5	3
MMCF-2	25	1	48	5.3	95.4	4
MOF-505	25	1	48	4	48.8	4
HKUST-1	25	1	48	4.1	49.2	4
MMPF-9	25	1	48	14.6	87.4	5
USTC-253-TFA	25	1	72	1.2	81.3	6
MIL-101(Cr)	25	8	24	10.3	82.0	7
Ba-(BDPO)	25	10	48	4.1	99.2	8
MOF-5	50	60	4	36.4	94.5	9
TbL	70	10	12	2.4	45.5	10
SmBTB	80	1	15	12.1	100	11
Cu <sub>2</sub> BPDSDC	80	25	5	19.1	99.0	12
Zeolite-β	120	7	3	16.0	100	13
UMCM-1-NH <sub>2</sub>	120	12	24	5.9	91.0	14
NH <sub>2</sub> -MIL-101(Al)	120	18	6	21.7	96.0	15

## References

1. K. C. Stylianou, J. E. Warren, S. Y. Chong, J. Rabone, J. Bacsa, D. Bradshaw and M. J. Rosseinsky, *Chemical Communications*, 2011, **47**, 3389-3391.
2. C. M. Simon, B. Smit and M. Haranczyk, *Computer Physics Communications*, 2016, **200**, 364-380.
3. D. H. Le, R. P. Loughan, A. Gładysiak, N. Rampal, I. A. Brooks, A.-H. A. Park, D. Fairen-Jimenez and K. C. Stylianou, *Journal of Materials Chemistry A*, 2022, **10**, 1442-1450.
4. W.-Y. Gao, Y. Chen, Y. Niu, K. Williams, L. Cash, P. J. Perez, L. Wojtas, J. Cai, Y.-S. Chen and S. Ma, *Angewandte Chemie International Edition*, 2014, **53**, 2615-2619.
5. W.-Y. Gao, L. Wojtas and S. Ma, *Chemical Communications*, 2014, **50**, 5316-5318.
6. Z.-R. Jiang, H. Wang, Y. Hu, J. Lu and H.-L. Jiang, *ChemSusChem*, 2015, **8**, 878-885.
7. O. V. Zalomaeva, A. M. Chibiryaev, K. A. Kovalenko, O. A. Kholdeeva, B. S. Balzhinimaev and V. P. Fedin, *Journal of Catalysis*, 2013, **298**, 179-185.
8. X.-Y. Li, L.-N. Ma, Y. Liu, L. Hou, Y.-Y. Wang and Z. Zhu, *ACS Applied Materials & Interfaces*, 2018, **10**, 10965-10973.
9. J. Song, Z. Zhang, S. Hu, T. Wu, T. Jiang and B. Han, *Green Chemistry*, 2009, **11**, 1031-1036.
10. T. Jing, L. Chen, F. Jiang, Y. Yang, K. Zhou, M. Yu, Z. Cao, S. Li and M. Hong, *Crystal Growth & Design*, 2018, **18**, 2956-2963.
11. B. Ugale, S. S. Dhankhar and C. M. Nagaraja, *Crystal Growth & Design*, 2018, **18**, 2432-2440.
12. F. Guo, *Journal of Molecular Structure*, 2019, **1184**, 557-561.
13. R. Srivastava, D. Srinivas and P. Ratnasamy, *Applied Catalysis A: General*, 2005, **289**, 128-134.
14. R. Babu, A. C. Kathalikkattil, R. Roshan, J. Tharun, D.-W. Kim and D.-W. Park, *Green Chemistry*, 2016, **18**, 232-242.
15. S. Senthilkumar, M. S. Maru, R. S. Somani, H. C. Bajaj and S. Neogi, *Dalton Transactions*, 2018, **47**, 418-428.